Redox Biology 19 (2018) 166–178

Contents lists available at ScienceDirect

Redox Biology

journal homepage: www.elsevier.com/locate/redox

Cinnamic aldehyde inhibits vascular smooth muscle cell proliferation and neointimal hyperplasia in Zucker Diabetic Fatty rats

Nicholas E. Buglak[a,b,c,1], Wulin Jiang[b,d,1], Edward S.M. Bahnson[a,b,c,e,*]

[a] Department of Surgery, Division of Vascular Surgery, University of North Carolina at Chapel Hill, NC 27599, USA
[b] Center for Nanotechnology in Drug Delivery, University of North Carolina at Chapel Hill, NC 27599, USA
[c] Curriculum in Toxicology & Environmental Medicine, University of North Carolina at Chapel Hill, NC 27599, USA
[d] Division of Pharmacoengineering and Molecular Pharmaceutics, University of North Carolina at Chapel Hill, NC 27599, USA
[e] Department of Cell Biology & Physiology, University of North Carolina at Chapel Hill, NC 27599, USA

ARTICLE INFO

Keywords:
Diabetes
Cinnamic aldehyde
Restenosis
Neointimal hyperplasia
Nrf2
Vascular smooth muscle cells

ABSTRACT

Atherosclerosis remains the number one cause of death and disability worldwide. Atherosclerosis is treated by revascularization procedures to restore blood flow to distal tissue, but these procedures often fail due to restenosis secondary to neointimal hyperplasia. Diabetes mellitus is a metabolic disorder that accelerates both atherosclerosis development and onset of restenosis. Strategies to inhibit restenosis aim at reducing neointimal hyperplasia by inhibiting vascular smooth muscle cell (VSMC) proliferation and migration. Since increased production of reactive oxygen species promotes VSMC proliferation and migration, redox intervention to maintain vascular wall redox homeostasis holds the potential to inhibit arterial restenosis. Cinnamic aldehyde (CA) is an electrophilic Nrf2 activator that has shown therapeutic promise in diabetic rodent models. Nrf2 is a transcription factor that regulates the antioxidant response. Therefore, we hypothesized that CA would activate Nrf2 and would inhibit neointimal hyperplasia after carotid artery balloon injury in the Zucker Diabetic Fatty (ZDF) rat. In primary ZDF VSMC, CA inhibited cell growth by MTT with an EC_{50} of 118 ± 7 μM. At a therapeutic dose of 100 μM, CA inhibited proliferation of ZDF VSMC *in vitro* and reduced the proliferative index within the injured artery *in vivo*, as well as migration of ZDF VSMC *in vitro*. CA activated the Nrf2 pathway in both ZDF VSMC and injured carotid arteries while also increasing antioxidant defenses and reducing markers of redox dysfunction. Additionally, we noted a significant reduction of neutrophils (69%) and macrophages (78%) within the injured carotid arteries after CA treatment. Lastly, CA inhibited neointimal hyperplasia evidenced by a 53% reduction in the intima:media ratio and a 61% reduction in vessel occlusion compared to arteries treated with vehicle alone. Overall CA was capable of activating Nrf2, and inhibiting neointimal hyperplasia after balloon injury in a rat model of diabetic restenosis.

1. Introduction

Cardiovascular disease (CVD) remains the number one cause of death and disability worldwide [1]. Atherosclerosis is the major underlying cause for most coronary and peripheral artery diseases. Diabetes mellitus (DM) is a series of metabolic disorders associated with a chronic state of hyperglycemia, systemic redox imbalance, inflammation, advanced glycation end products, dyslipidemia, and endothelial dysfunction. DM patients are two to three times more likely to have CVD than non-diabetics [2] and exhibit an increased rate of atherosclerotic plaque development [3]. Revascularization procedures for occluded arteries include balloon angioplasty with or without stent placement. The arterial injury response after revascularization often results in vessel re-occlusion, or restenosis, which in turn requires

Abbreviations: ARE/EpRE, antioxidant/electrophile response element; BrdU, bromodeoxyuridine; CA, cinnamic aldehyde; CVD, cardiovascular disease; DHE, dihydroethidium; DM, diabetes mellitus; GCLC, glutamate-cysteine ligase catalytic subunit; GSH, glutathione; HO-1, heme oxygenase-1; I:M, intima:media; MPO, myeloperoxidase; NOX1, NADPH oxidase 1; Nrf2, nuclear factor erythroid 2-related factor 2; PDGF, platelet derived growth factor; Prx, peroxiredoxin; ROS, reactive oxygen species; SFN, sulforaphane; SOD, superoxide dismutase; VSMC, vascular smooth muscle cells; XO, xanthine oxidase; ZDF, Zucker Diabetic Fatty rat

* Corresponding author at: Center for Nanotechnology in Drug Delivery, University of North Carolina at Chapel Hill, 125 Mason Farm Rd, Chapel Hill, NC 27599, USA.
E-mail address: edward_bahnson@med.unc.edu (E.S.M. Bahnson).
[1] These authors contributed equally to this work.

https://doi.org/10.1016/j.redox.2018.08.013
Received 19 July 2018; Received in revised form 15 August 2018; Accepted 22 August 2018
Available online 24 August 2018

further intervention. DM also accelerates restenosis as evidenced by lower patency rates after revascularization in diabetic patients [4–6].

Restenosis is secondary to vessel constrictive remodeling and neointimal hyperplasia, or the inward migration and proliferation of both vascular smooth muscle cells (VSMC) [7] from the media and fibroblasts from the adventitia [8] into the intima. Drug-eluting stents are currently the most effective therapy for restenosis as they inhibit all cellular proliferation and migration within the vessel, but their use increases the risk of thrombosis by preventing vessel reendothelialization [9]. Thus, emerging therapies aim to prevent the proliferation and migration of VSMC and fibroblasts after injury without inhibiting endothelialization.

Local redox imbalance has been described as a major contributing factor for this VSMC pathology [10,11]. Specifically, reactive oxygen species downstream of NADPH oxidase 1 (NOX1), superoxide and subsequently hydrogen peroxide, are overproduced after injury and promote VSMC growth and migration [12–15]. Additionally, the family of platelet derived growth factors (PDGF) have been implicated as one of the major growth signals upstream of NOX1 [16]. Small molecules that target the redox imbalance have shown promise as potential therapeutics for preventing the VSMC phenotypic changes [17–19]. A novel therapeutic approach is to restore the redox balance by activating nuclear factor erythroid 2-related factor 2 (Nrf2), the main antioxidant defense pathway present in our cells [20,21]. Indeed, treatment with sulforaphane, a Nrf2 activating small molecule, has been shown to inhibit restenosis in a non-diabetic Sprague Dawley rat balloon injury model [22] as well as wire injured mouse models [23,24]. To date, however, no study has evaluated the efficacy of these small molecules in a diabetic model of restenosis.

Cinnamic aldehyde (CA) is an α,β-unsaturated aldehyde extracted from cinnamon that activates Nrf2 [25,26]. CA has been shown to prevent hyperglycemia-induced endothelial dysfunction [27], be protective against diabetes-induced hypertension in rats [28], and exhibit overall anti-diabetic effects [29]. We hypothesized that CA would inhibit neointimal hyperplasia in a diabetic restenosis model. Accordingly, we used Zucker Diabetic Fatty (ZDF) rats, a well characterized type 2 DM model, for our *in vitro* and *in vivo* evaluation. Primary aortic ZDF VSMC were treated in the presence of high glucose (25 mM) and PDGF-BB (25 ng/mL) as an *in vitro* model of injury in diabetes. We used the carotid artery balloon injury in the ZDF rats after onset of diabetes to evaluate the therapeutic potential of CA at inhibiting neointimal hyperplasia formation.

2. Materials and methods

2.1. Materials

Cinnamic aldehyde (CA) (C80687; Sigma-Aldrich, St. Louis, MO). DMEM (11885-084; Gibco, Grand Island, NY). DMSO (BP231; Thermo-Fisher Scientific, Waltham, MA). F-12 (11765-054; Gibco). Glucose (50-99-7, Sigma-Aldrich). Heat-inactivated fetal bovine serum (FBS) (16140071; Gibco). Paraformaldehyde (158127; Sigma-Aldrich). PBS (20–134; Apex Bioresearch Products, San Diego, CA). Sulforaphane (SFN) (S6317; Sigma-Aldrich). Trypsin-EDTA (0.05%) (25300054; Gibco).

2.2. Animals

All animal handling and experimental procedures were approved by the Institutional Animal Care and Use Committee at the University of North Carolina – Chapel Hill. (Ref no. IACUC16-254 (10-2016-09-2019)). Male Zucker Diabetic Fatty (ZDF) rats were obtained from Charles River Laboratories (Wilmington, MA). Animals were fed Irradiated Purina 5008 (Granville Milling, Granville, OH) chow. Blood glucose was measured by tail nick using a Freestyle Precision Neo Blood Glucose Monitoring System (Abbott Laboratories, Abbott Park, Illinois). Glycemia > 400 mg/dL after two consecutive random weekly measurements was used to determine type 2 diabetes onset.

2.3. Rat carotid artery injury model

Adult male ZDF rats weighing 350–500 g were used for surgery after onset of diabetes. Rats were anesthetized with inhaled isoflurane (0.5–2%). Atropine (0.1 mg/kg) was administered subcutaneously (SC) to reduce airway secretions and Carprofen (5 mg/Kg) was administered SC for pain management. After a sterile prep and midline neck incision, the left common, internal, and external carotid arteries were dissected and the internal and common carotid arteries were occluded. A No. 2 French Fogarty balloon catheter (Edwards Lifesciences, Irvine, CA) was inserted through an arteriotomy in the external carotid artery and advanced into the common carotid artery. The balloon was inflated to 5 atm of pressure for 5 min to create a uniform injury. After removal of the balloon, the external carotid artery was ligated and blood flow was restored. 100 μM CA was applied in 100 μL of Pluronic-127 (P2443; Sigma-Aldrich) gel periadventitially to the external surface of the injured common carotid artery and then the neck incision was closed. Two separate cohorts of rats, one from each of the two surgeons that performed the model, were sacrificed 2 weeks (total n = 6/group) after surgery for morphometric analysis of neointimal hyperplasia and macrophage presence. Rats were sacrificed 3 days after surgery for analyzing proliferation, redox biomarker levels, and inflammatory cell invasion. To analyze cell proliferation, bromodeoxyuridine (BrdU) (B5002; Sigma-Aldrich) was administered via intraperitoneal injection 1 day and 1 h prior to euthanasia. One vehicle-treated, 3-day injury rat was not included in analysis due to thrombus development in the common carotid artery.

2.4. Tissue processing

Carotid arteries were harvested after in situ perfusion-fixation with 200 mL of PBS and 200 mL of cold 2% paraformaldehyde. Arteries were placed in 2% paraformaldehyde for 1 h at 4 °C followed by 30% sucrose overnight at 4 °C. Arteries were quick-frozen in O.C.T. (4583; Tissue-Tek, Torrance, CA) and stored at − 80 °C. 5 μm sections were cut throughout the entire common carotid artery for staining.

2.5. Histological and Immunofluorescence analysis

Immunofluorescent (IF) staining for 3-day injured arteries (n = 5 vehicle alone; n = 6 CA-treatment): 10 μM dihydroethidium (DHE) (D23107, Thermo-Fisher Scientific) diluted in DMSO for 10 min in the dark; 1:1000 anti-3-nitrotyrosine antibody (ab61392; Abcam, Cambridge, UK) in IHC-Tek diluent (1W-1000; IHC World, Woodstock, MD) for 1 h followed by 1:1000 Alexa Fluor 555 goat anti-mouse IgG (A-21236, Invitrogen, Carlsbad, CA) in PBS for 1 h; 1:100 anti-myeloperoxidase (ab9535; Abcam) in IHC-Tek diluent for 1 h after permeabilization with 0.3% Triton X-100 (X100; Sigma-Aldrich) followed by 1:100 Alexa Fluor 647 goat anti-rabbit IgG (A21245; Invitrogen) in PBS for 1 h; 1:1000 anti-CD68 (MCA341R; Bio-Rad, Hercules, CA) in IHC-Tek diluent for 1 h followed by 1:500 Alexa Fluor 647 goat anti-mouse IgG (A-21236; Invitrogen) in PBS for 1 h; counterstain with 0.6 μM DAPI (D3571; Invitrogen) diluted 1:500 in PBS for 5 min was performed with all immunofluorescent staining. ProLong Gold Antifade Reagent (P36930, Thermo-Fisher Scientific) was used for mounting coverslips. 3-day injured arteries were stained for BrdU uptake according to the manufacturer's instructions (ab125306; Abcam). 2-week injured arteries were H&E stained for measuring neointimal hyperplasia and IF stained for CD68. For *in vitro* IF, after 24 h treatment with 100 μM CA or 4 μM SFN, VSMC were stained with 10 μM DHE for 1 h followed by 0.6 μM DAPI diluted 1:500 in PBS for 5 min. Slides were imaged on the day after staining using a Zeiss Axio Imager. A2 microscope (Oberkochen, Germany). Images were taken on a 5x objective for

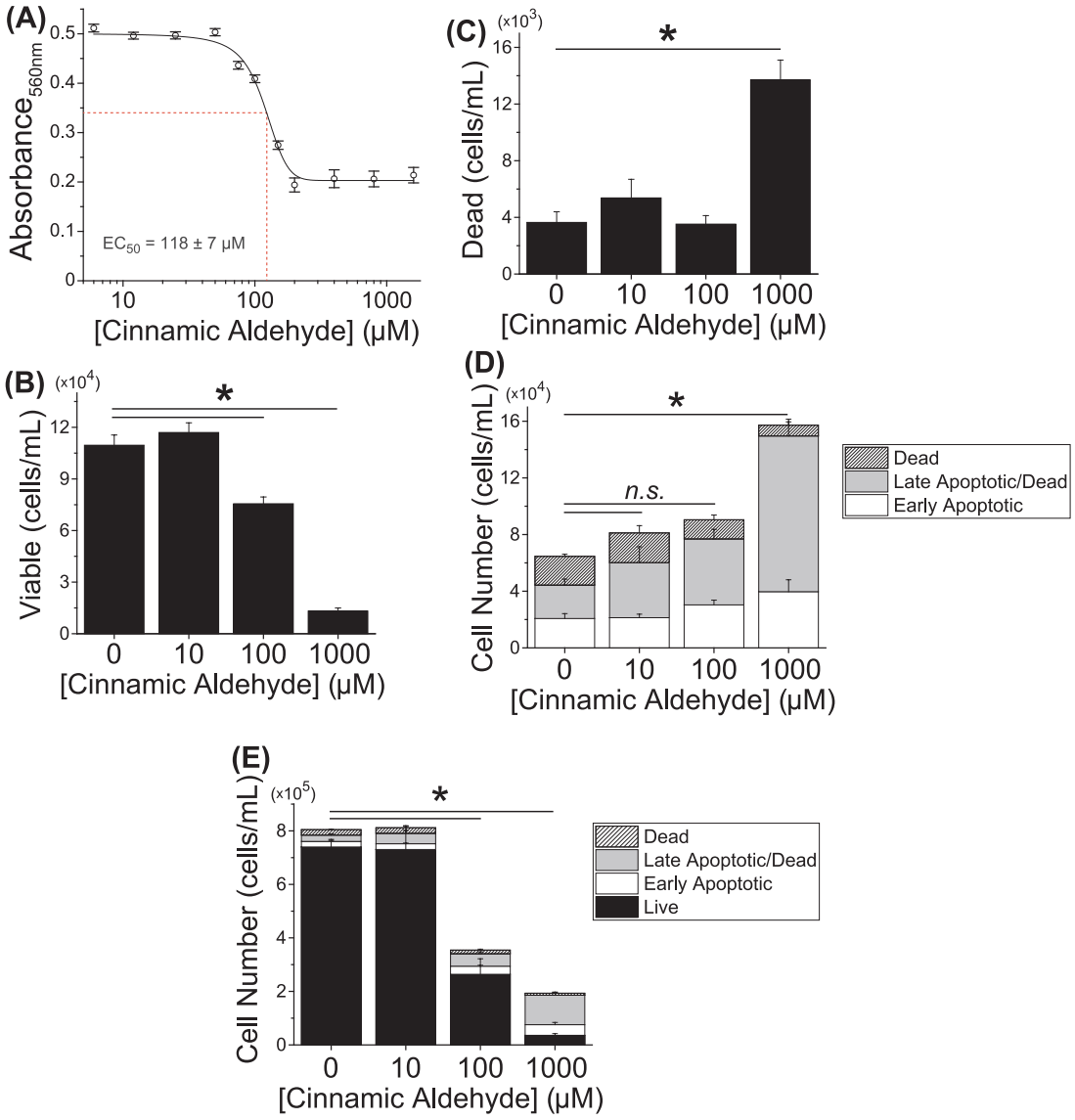

Fig. 1. 100 μM cinnamic aldehyde (CA) reduced PDGF-BB-stimulated ZDF vascular smooth muscle cell (VSMC) number without inducing apoptosis. ZDF VSMC in 25 mM glucose were synchronized overnight and then stimulated with 25 ng/mL PDGF-BB for 24 h with or without varying concentrations of CA. (A) Metabolic activity analyzed by MTT of ZDF VSMC treated with CA dose range (EC50 = 118 ± 7 μM) (n = 3 independent experiment with 8 replicates). (B) Quantification of total viable ZDF VSMC after treatment with increasing doses of CA. (C) Quantification of total dead ZDF VSMC after CA treatment. (D) Quantification of early apoptotic, late apoptotic, and dead ZDF VSMC after treatment with increasing doses of CA. Significant increase shown is only in the late apoptotic cell population. No significant change in other subpopulations. (E) Live subpopulation of ZDF VSMC included with subpopulations from (D) with significant decrease in total cell number at 100 μM and 1000 μM CA shown. (B-E) *$p < 0.05$ compared to control (0 μM CA); one-way ANOVA with post hoc Tukey's correction for multiple comparisons. Data presented as means ± SEM (n = 3 independent experiments in triplicate).

quantification and a 20x objective for representative figures. Filters were selected for each fluorescent probe as follows: ex = 365 nm, em = 445/50 nm for DAPI; ex = 545/25 nm, em = 605/50 nm for Alexa 555 and DHE; and ex = 640/30 nm, em = 690/50 nm for Alexa 647. All staining was quantified using ImageJ software (https://imagej.nih.gov/ij/). For BrdU stained arteries (n = 5 vehicle alone; n = 8 CA-treatment) blue cells were identified as BrdU negative, or non-proliferating, and brown cells as BrdU positive, or proliferating cells. Final proliferative index (BrdU-positive/total cells) for each animal was quantified by averaging the index from three to five evenly-spaced arterial sections. Neointimal hyperplasia was quantified using ImageJ by tracing the areas of the outer elastic lamina, inner elastic lamina, and neointima. An intima: media (I:M) ratio and a percent occlusion were calculated as follows: $I:M = Area_{intima}/Area_{media}$; $\%\ Occlusion = (1–((Area_{lumen}-Area_{intima})/Area_{lumen})) \times 100$.

2.6. Confocal microscopy

Cells and tissue were stained for Nrf2 as described above. Slides were imaged with a Nikon A1R laser scanning confocal microscope (Melville, NY) with the appropriate excitation wavelengths for green (Ex = 488 nm), red (Ex = 561 nm), and blue (Ex = 405 nm). Optical slices were captured at regular intervals to produce reconstructed z-stacks. Single-plane and 3D reconstructions were obtained using Nikon Elements software.

2.7. Cell culture

Primary vascular smooth muscle cells (VSMC) were isolated from the thoracic aorta of 10–12-week male ZDF rats as previously described [30]. ZDF VSMC used between passages 4–9 for all experiments. ZDF VSMC were cultured in an incubator at 37 °C with 5% CO_2. VSMC were

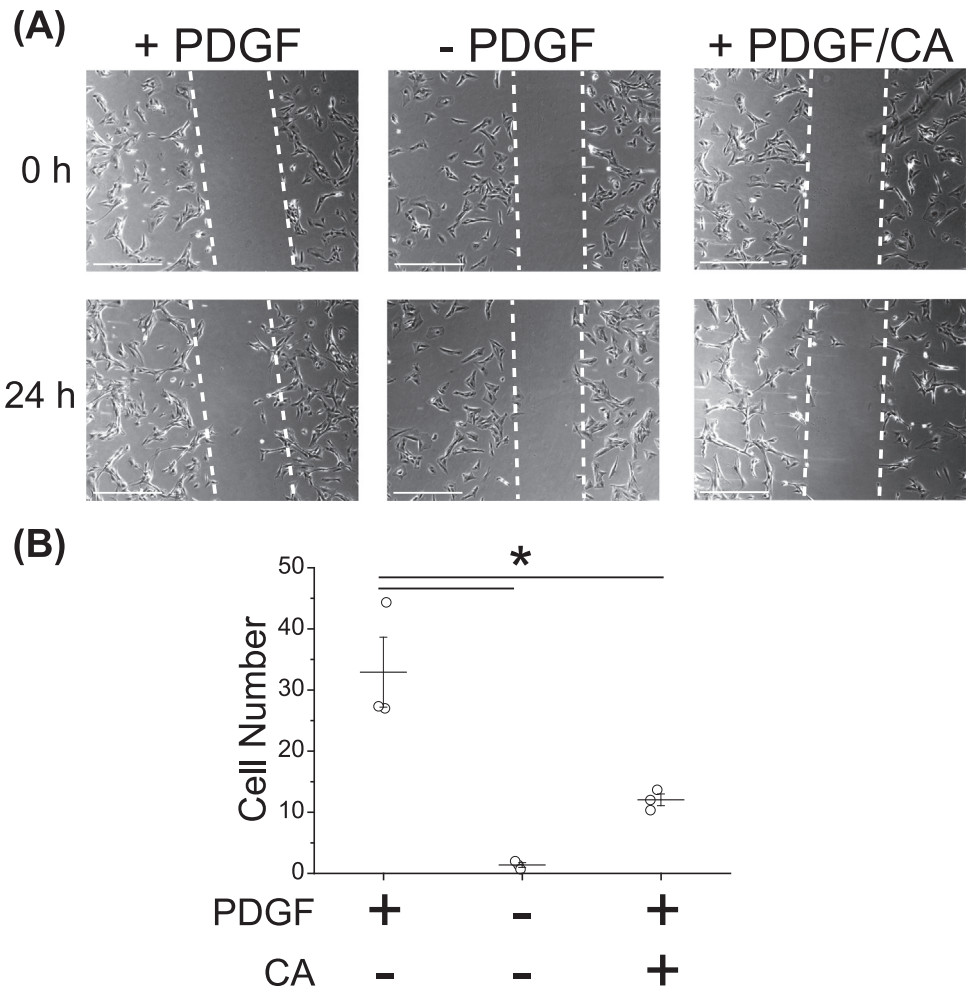

Fig. 2. Cinnamic aldehyde (CA) inhibited PDGF-BB-induced ZDF vascular smooth muscle cell (VSMC) migration. ZDF VSMC in 25 mM glucose were synchronized overnight and then stimulated with 25 ng/mL PDGF-BB for 24 h with or without varying concentrations of CA. (A) Phase contrast images of PDGF-treated (+), PDGF-starved (-), and 100 μM CA treated ZDF VSMC at 0 and 24 h. Scale bar = 500 μm. (B) Quantification of migratory ZDF VSMC within the scratch area as indicated by the dashed lines in (A). *$p < 0.05$ compared to PDGF-treated control; one-way ANOVA with Tukey's correction. Data presented as means ± SEM (n = 3 independent experiments in triplicate).

maintained in low glucose (4 mM) 1:1 DMEM:F-12 media supplemented with 10% FBS. For assays the cells were seeded in high glucose (25 mM) DMEM:F-12 media, synchronized through serum-starvation in high glucose, and treated for assays in high glucose media supplemented with 25 ng/mL platelet derived growth factor–BB (PDGF-BB) (P4056; Sigma-Aldrich). CA was stored in air-displaced amber vials at room temperature and diluted in DMSO prior to serial dilution in media for treatment. SFN was stored at − 20 °C and diluted directly in media for treatment. Equal volume DMSO was included for all controls.

2.8. Western blot analysis

Synchronized ZDF VSMC in 6-well plates (seeded at 2×10^5 cells/well) were treated for 4, 6, or 24 h with 100 μM CA or 4 μM SFN and cell pellets were obtained by trypsinization for whole cell lysate or by scraping for nuclear/cytoplasmic lysates. Nuclear extracts obtained following manufacturer's protocol (40010; Active Motif, Carlsbad, CA). Protein quantification by BCA assay (23225; Thermo-Fisher Scientific). 10 μg of protein was loaded in a 4% stacking/13% running homecast gel, following Bio-Rad protocol (bulletin 6040). Gel was transferred to and blotted for protein on a PVDF membrane (10600023; GE Life Sciences, Pittsburgh, PA). Near Infrared Blocking Buffer (RLMB-070; Rockland Immunochemicals, Pottstown, PA) was used for all protein probing. Primary antibodies used at dilutions of 1:1000 of anti-Nrf2 antibody (ab137550; Abcam), 1:500 of anti-heme oxygenase 1 antibody (ADI-OSA-110-F; Enzo Life Sciences, Farmingdale, NY), 1:1000 of anti-glutamate-cysteine ligase catalytic subunit antibody (ab190685; Abcam), 1:1000 of anti-peroxiredoxin 1 (ab16805-100; Abcam), 1:1000 of anti-peroxiredoxin 3 (ab73349; Abcam), 1:1000 of anti-superoxide dismutase 1 antibody (ab13499; Abcam), 1:2000 of anti-TATA binding protein antibody (ab818; Abcam), or 1:15000 of anti-β-actin antibody (A5441; Sigma-Aldrich). Secondary antibodies used at dilutions of 1:5000 for anti-rabbit (926–32211; LI-COR Biosciences, Lincoln, NE) or 1:2000–1:10,000 for anti-mouse (926-68070; LI-COR Biosciences) antibody. Membranes were imaged using LI-COR Odyssey 9120 Infrared Imaging System (LI-COR Biosciences). Band intensity relative to β-actin or TATA binding protein was quantified using ImageJ software.

2.9. Cell migration assay

Scratch wound assay was performed on synchronized ZDF VSMC in a 12-well plate at 70% confluency and cells were treated with 100 μM CA. Wells were imaged at time of scratch and 24 h later using Gen 5 software (BioTek Instruments, Winooski, VT) on a Cytation 5 plate reader (BioTek Instruments). Migratory cells within the scratch region were quantified using ImageJ software.

2.10. MTT assay

ZDF VSMC (5×10^3 cells/well) were seeded in 96-well plates. Synchronized ZDF VSMC were treated with a range [6–1600 μM] of CA for 24 h. ZDF VSMC were treated with 0.4 mg/mL Thiazolyl Blue tetrazolium bromide (L11939; Alfa Aesar, Haverhill, MA) diluted in low glucose FBS-supplemented complete media for 4 h at 37 °C. After treatment, media was removed and plates were left to air-dry overnight. Formazan crystals were resuspended in DMSO and absorbance was measured at 560 nm with background at 670 nm on a Cytation 5 plate reader.

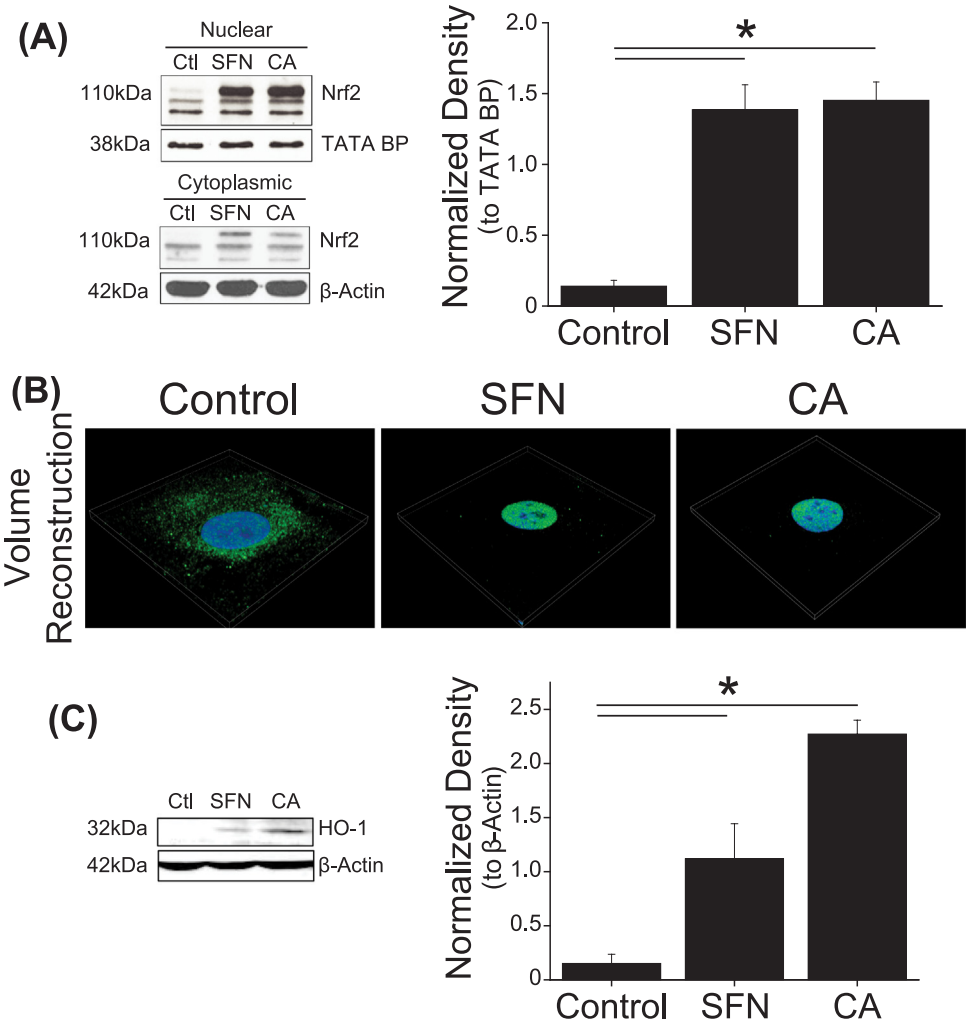

Fig. 3. Cinnamic aldehyde (CA) activated the Nrf2 pathway in ZDF vascular smooth muscle cells (VSMC). (A-C) ZDF VSMC in 25 mM glucose were synchronized overnight and then stimulated with 25 ng/mL PDGF-BB with or without varying concentrations of CA. (A) Immunoblot of nuclear and cytoplasmic ZDF VSMC fractions treated with 100 μM CA or 4 μM sulforaphane (SFN) for 6 h probed for Nrf2 with TATA Binding Protein (TATA BP) or β-Actin in the nuclear and cytoplasmic fraction respectively. Plot of nuclear fraction Nrf2 band density normalized to TATA BP. (B) Confocal images of subcellular Nrf2 localization after CA or SFN treatment for 24 h. Green = Nrf2; Blue = Nuclei. (C) Representative immunoblot of whole cell lysates treated with CA or SFN for 4 h probed for heme oxygenase 1 (HO-1). Plot of HO-1 band density normalized to β-Actin (n = 3). (D) Hyperglycemic ZDF rats weighing 350–500 g underwent the carotid balloon injury and were treated with periadventitial application of Pluronic vehicle (100 μL) or CA in Pluronic (100 μM in 100 μL) at the time of surgery. Carotids were harvested three days after surgery. Confocal images of three-day injured carotid arteries stained for Nrf2. Red = Nrf2; Blue = DAPI; Green = elastic lamina; L = lumen. Arrows indicate nuclear co-localization. *p < 0.05 compared to control (Ctl); one-way ANOVA with Tukey's correction. Data presented as means ± SEM (n = 3 independent experiments in triplicate; n = 3 ZDF VSMC or tissue cross-sections for confocal images with representative image shown).

2.11. Cell viability assay

ZDF VSMC (5×10^4 cells/well) were seeded in 12-well plates. Synchronized ZDF VSMC were treated with 10 μM, 100 μM, or 1 mM CA for 24 h. Cells were collected using trypsin, pelleted by centrifugation (300 × *g*, 5 min), and stained using the manufacturer's instructions (MCH100102, Sigma-Aldrich). Viability was quantified for each well using Muse Cell Analyzer (MilliporeSigma, Burlington, MA).

2.12. Cell apoptosis assay

ZDF VSMC (5×10^4 cells/well) were seeded in 12-well plates. Synchronized ZDF VSMC were treated with 10 μM, 100 μM, or 1 mM CA for 24 h. Cells were collected using trypsin, pelleted by centrifugation (300 × *g*, 5 min), and stained using the manufacturer's instructions (MCH100105, Sigma-Aldrich). Live, early apoptotic, late apoptotic, and dead cells were quantified for each well using Muse Cell Analyzer. Each proportion was determined by the appropriate combination of negative or positive staining for Annexin V and 7-Aminoactinomycin D.

2.13. Superoxide dismutase activity assay

ZDF VSMC (2×10^5 cells/well) were seeded in 6-well plates. Synchronized ZDF VSMC were treated with 100 μM CA or 4 μM SFN for 24 h. Cells were collected by gentle scraping on ice, pelleted by centrifugation (1000 × *g*, 5 min, 4 °C), and lysed without the use of protease inhibitors. Superoxide dismutase (SOD) activity assay was performed according to the manufacturer's instructions (706002, Cayman

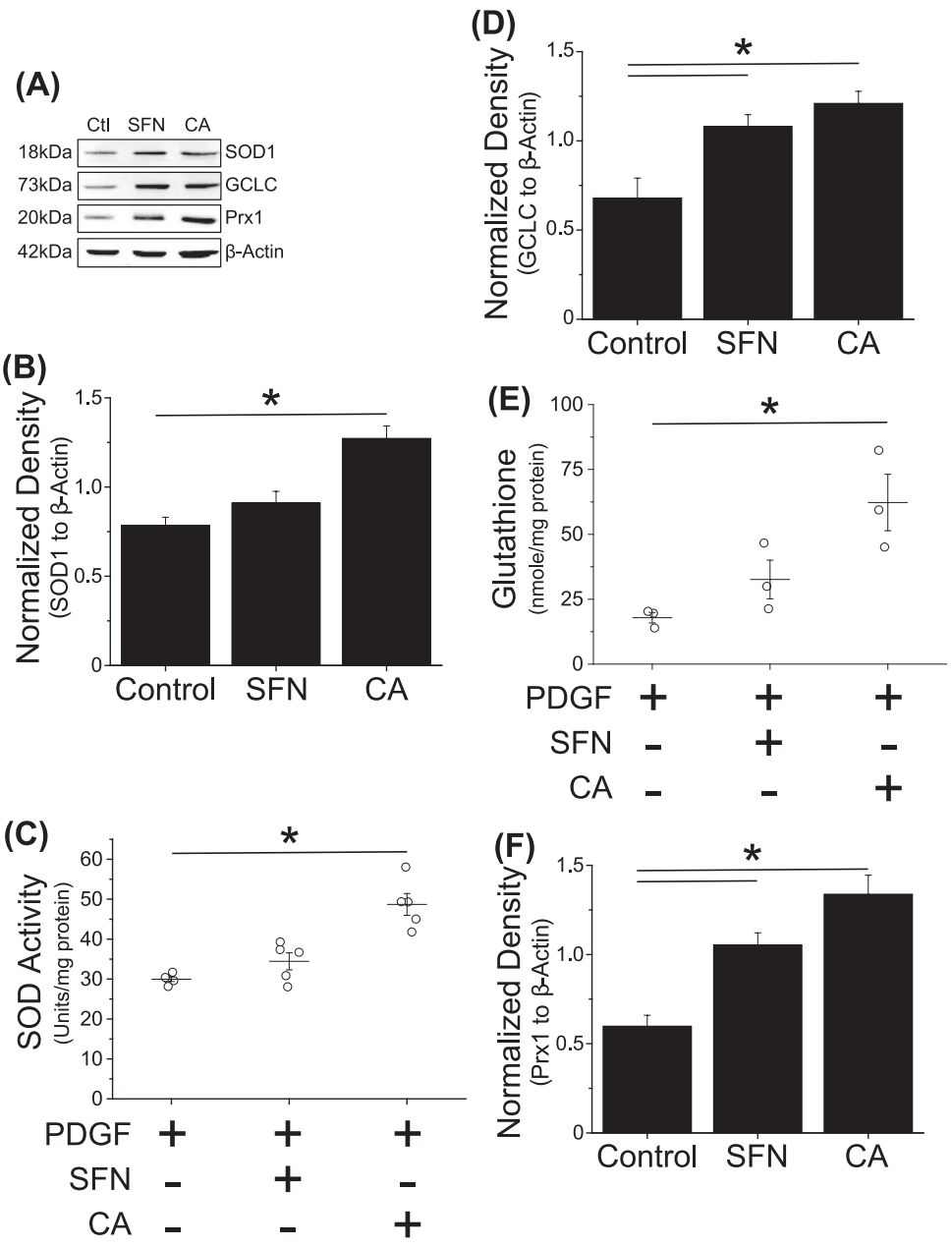

Fig. 4. Cinnamic aldehyde (CA) increased antioxidant levels in ZDF vascular smooth muscle cells (VSMC). ZDF VSMC in 25 mM glucose were synchronized overnight and then stimulated with 25 ng/mL PDGF-BB with or without 100 μM CA or 4 μM sulforaphane (SFN) for 24 h. (A) Representative immunoblot of whole cell lysates probed for superoxide dismutase 1 (SOD1), glutamate-cysteine ligase catalytic subunit (GCLC), peroxiredoxin 1 (Prx1), and β-Actin. (B) Plot of SOD1 band density normalized to β-Actin (n = 3). (C) Total SOD activity in treated ZDF VSMC (n = 5 with technical duplicates). (D) Plot of GCLC band density normalized to β-Actin (n = 3). (E) Intracellular glutathione levels in treated ZDF VSMC (n = 3 with technical duplicates). (F) Plot of Prx1 band density normalized to β-Actin (n = 3). (B-F) *p < 0.05 compared to control (Ctl); Data analyzed with one-way ANOVA with Tukey's correction. Data presented as means ± SEM.

Chemical, Ann Arbor, MI) in an acrylic UV 96-well plate. Following the addition of xanthine oxidase the plate was placed on a shaker for 30 min at room temperature. Absorbance was measured at 450 nm using Cytation 5 plate reader. Total SOD activity was reported as Units/mg protein.

2.14. Glutathione assay

ZDF VSMC (2×10^5 cells/well) were seeded in 6-well plates. Synchronized ZDF VSMC were treated with 100 μM CA or 4 μM SFN for 24 h. Cells were collected by gentle scraping on ice, pelleted by centrifugation (1000 × *g*, 5 min, 4 °C), and lysed without the use of protease inhibitors. Total glutathione (GSH) was quantified according to the manufacturer's instructions (703002, Cayman Chemical) in an acrylic UV 96-well plate utilizing the reaction between GSH and DTNB (5,5′-Dithio-*bis*-(2-nitrobenzoic acid)). Plate was placed on a shaker for 25 min at room temperature and then absorbance was measured at 414 nm using Cytation 5 plate reader. GSH levels were reported in nmole/mg protein.

2.15. Statistical analysis

Numerical data are represented as means ± SEM. Statistical analyses were performed using an unpaired Student's *t*-test or one-way ANOVA, followed by Tukey's post-hoc test, as appropriate with a *p*-value < 0.05 considered statistically significant (OriginLab, Northampton, MA).

3. Results

3.1. Cinnamic aldehyde inhibits PDGF-induced VSMC proliferation

Since neointimal hyperplasia results from the abnormal proliferation and migration of VSMC, it is critical to evaluate the inhibitory ability of CA on these parameters. Therefore, we first assessed the effect of CA on PDGF-BB-treated ZDF VSMC viability. Using the MTT assay to measure metabolic activity following treatment we identified 118 ± 7 μM as the EC_{50} for CA in the ZDF VSMC (Fig. 1 A). Flow cytometry analysis determined that the total viable cell number following

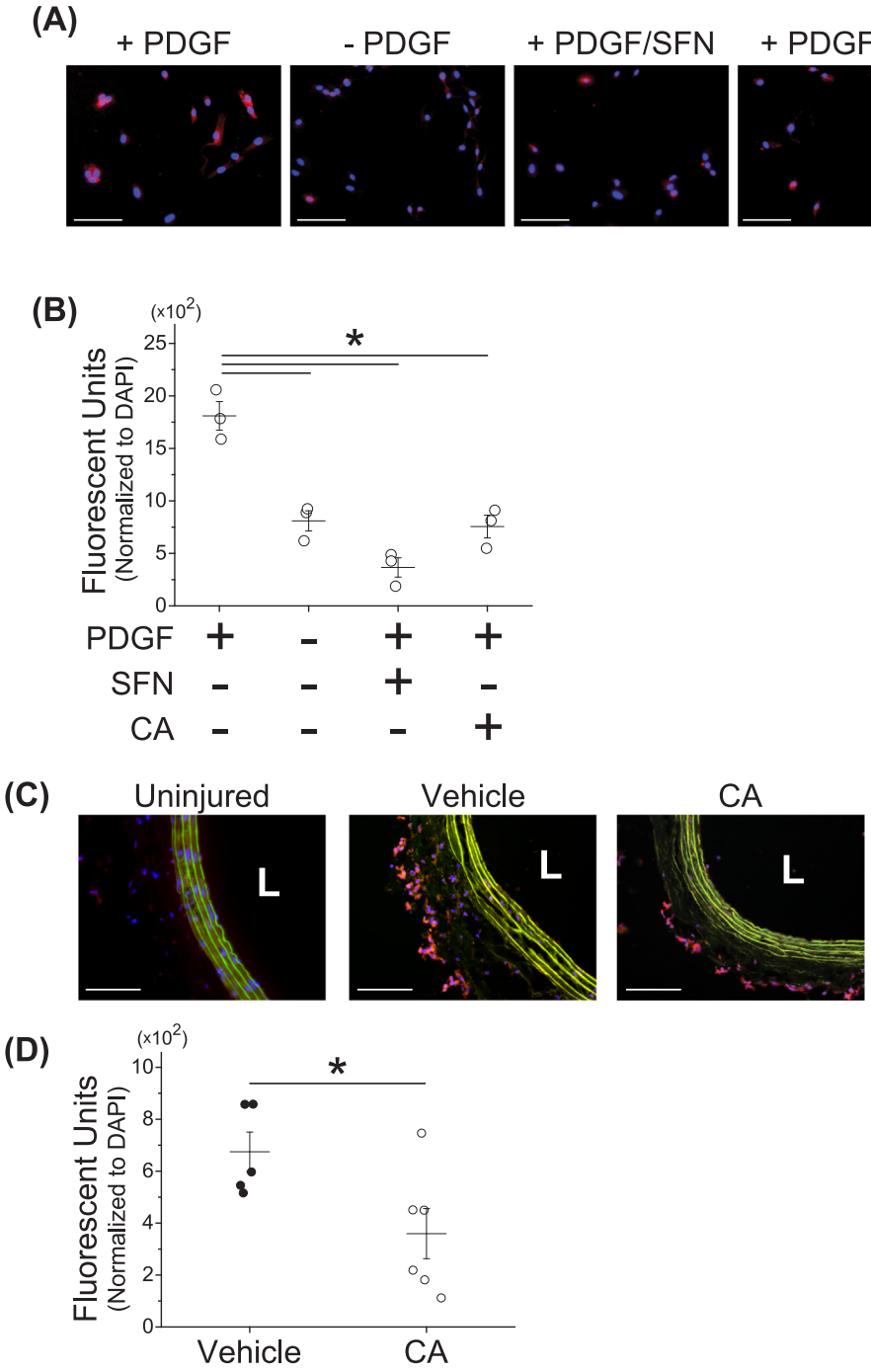

Fig. 5. Cinnamic aldehyde (CA) reduced levels of redox markers in ZDF vascular smooth muscle cells (VSMC) and injured carotid arteries. (A-B) ZDF VSMC in 25 mM glucose were synchronized overnight then treated for 24 h with or without stimulation by 25 ng/mL PDGF-BB in the presence of either CA (100 μM) or sulforaphane (SFN) (4 μM). (A) Representative images of ZDF VSMC stained with dihydroethidium (DHE). Scale bar = 100 μm; Red = DHE; Blue = DAPI. (B) Quantification of fluorescence from images in (A) normalized to cell nuclear count (DAPI). (C-F) Hyperglycemic ZDF rats weighing 350–500 g underwent the carotid balloon injury and were treated with periadventitial application of Pluronic vehicle (100 μL) or CA in Pluronic (100 μM in 100 μL) at the time of surgery. Carotids were harvested three days after surgery. (C) DHE staining of uninjured or three-day injured carotid arteries treated with 100 μM CA or vehicle alone. Scale bar = 100 μm; Red = DHE; Blue = DAPI; Green = elastic lamina; L = lumen. (D) Quantification of fluorescence from images in (C) normalized to cell nuclear count. (E) Immunofluorescent images for 3-nitrotyrosine staining of three-day injured carotid arteries. Scale bar = 100 μm; Red = 3-nitrotyrosine; Blue = DAPI; Green = elastic lamina; L = lumen. (F) Quantification of fluorescence from images in (E). (B) *$p < 0.05$ compared to PDGF-alone control. Data presented as means ± SEM (n = 3 independent experiments in triplicate). (D, F) *$p < 0.05$ compared to vehicle alone. One-way ANOVA with post hoc Tukey's correction for multiple comparison. Each point indicates the average of three arterial cross-sections per rat (n = 5 for vehicle, n = 6 for CA) with means ± SEM for each group overlaid.

CA treatment was reduced in a dose dependent manner. Treatment with 100 μM CA significantly reduced the total viable cell number ($p < 0.05$, Fig. 1 B) without increasing the total number of dead cells (p = NS compared to control, Fig. 1 C). Treatment with 1 mM CA, however, did increase cell death suggesting high dose CA toxicity ($p < 0.05$, Fig. 1C).

Next, apoptosis analysis was performed to investigate if the observed reduction in viable cell number was through CA-induced ZDF

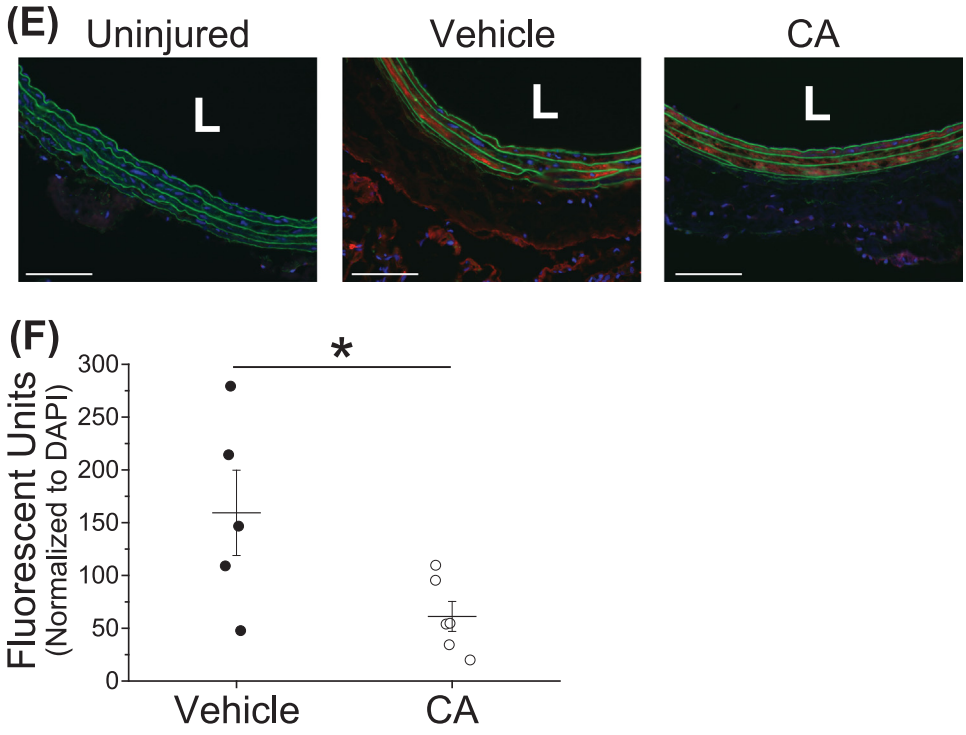

Fig. 5. (*continued*)

VSMC apoptosis. Flow cytometry results showed that 10 μM and 100 μM CA treatment did not increase either the total apoptotic cell population or the proportion of early apoptotic, late apoptotic, or dead cell subpopulations within the apoptotic cell population (p = NS, Fig. 1 D). Meanwhile, the increased cell death following 1 mM CA treatment was primarily attributed to the larger proportion of late apoptotic cells. When the live cell population was included in the analysis there was a significant decrease in total cell number at 100 μM CA, similarly to the findings from the viability assay ($p < 0.05$, Fig. 1 E). Taken together, these results suggest that low concentration CA reduced PDGF-BB-treated ZDF VSMC total cell number by inhibiting cell proliferation, while cell apoptosis contributed more to the reduction in total ZDF VSMC number only at toxic CA concentrations.

3.2. Cinnamic aldehyde inhibits PDGF-induced VSMC migration

Next, we investigated the inhibitory effect of CA on PDGF-BB-induced ZDF VSMC migration using the scratch wound assay. 100 μM CA significantly inhibited ZDF VSMC migration (Fig. 2 A). The number of migratory cells within the scratched region was reduced after CA treatment with an average of 12 migratory cells / field compared to 33 cells / field in the PDGF-BB-alone group ($p < 0.05$, Fig. 2 B). This suggests that along with proliferation CA also effectively inhibits ZDF VSMC migration.

3.3. Cinnamic aldehyde activates the Nrf2 pathway in ZDF VSMC and injured arteries

Nrf2 is the key transcription factor regulating the antioxidant response within cells [20]. The activation of the Nrf2 pathway leads to its nuclear translocation from the cytoplasm and consequentially its binding with the antioxidant/electrophile response element motif (ARE/EpRE) of cytoprotective genes [21], such as heme-oxygenase 1 (HO-1). Therefore, we set out to investigate whether CA activates the Nrf2 pathway in our ZDF VSMC. We used sulforaphane (SFN) as a positive control in our *in vitro* probing as it is a well characterized Nrf2-activator [31] that has been shown to inhibit neointimal hyperplasia [22]. After a 6-h treatment with 100 μM CA, the Nrf2 level in the nuclei of ZDF VSMC significantly increased to the same level as the ZDF VSMC treated with 4 μM SFN ($p < 0.05$, Fig. 3 A). Nrf2 nuclear translocation was further validated by confocal microscopy (Fig. 3 B). 4-h treatment significantly increased HO-1 levels in whole cell lysates in both the CA and SFN groups, at 15-fold and 7-fold increases respectively ($p < 0.05$, Fig. 3 C). This suggests the Nrf2 nuclear translocation results in the activation of its downstream signaling pathway.

Next, we imaged for Nrf2 activation within the carotid artery of balloon-injured rats. 100 μM CA was applied periadventitially in 100 μL of Pluronic gel to the injured left carotid artery at the time of balloon injury surgery. Carotids were obtained three days after injury and Nrf2 localization was assessed by confocal microscopy. Staining of the arterial cross-sections showed co-localization of Nrf2 with VSMC nuclei only after CA treatment, with diffuse staining seen in the vehicle-alone group (Fig. 3 D). Together this suggests that CA activates Nrf2 both *in vitro* and *in vivo*.

3.4. Cinnamic aldehyde increases antioxidant defenses in vitro and reduces markers of redox dysfunction both in vitro and in vivo

Local redox imbalance, specifically overproduction of superoxide, at the site of vascular injury drives neointimal hyperplasia [10]. Superoxide dismutase 1 (SOD-1) expression, transcriptionally controlled by Nrf2 [32], has been shown to regulate VSMC superoxide levels [30]. Hence, we assessed the levels of SOD-1 protein and noted a 1.6-fold increase in SOD-1 after 24-h CA treatment ($p < 0.05$, Fig. 4 A, B). Furthermore, ZDF VSMC treated for 24 h with CA exhibited 1.6-fold increased total SOD activity compared to untreated controls ($p < 0.05$, Fig. 4 C). Next, we measured glutamate-cysteine ligase catalytic subunit (GCLC) levels as GCLC is transcriptionally regulated by Nrf2 and involved in the synthesis of glutathione (GSH), the major intracellular antioxidant. 24-h treatment with both CA and SFN increased the levels of GCLC 1.8-fold and 1.6-fold respectively ($p < 0.05$, Fig. 4 A, D). Concurrently, the ZDF VSMC had a 3.5-fold increase in intracellular GSH after 24-h CA treatment ($p < 0.05$, Fig. 4 E). Lastly, we measured the levels of peroxiredoxin 1 (Prx1), an enzyme also transcriptionally

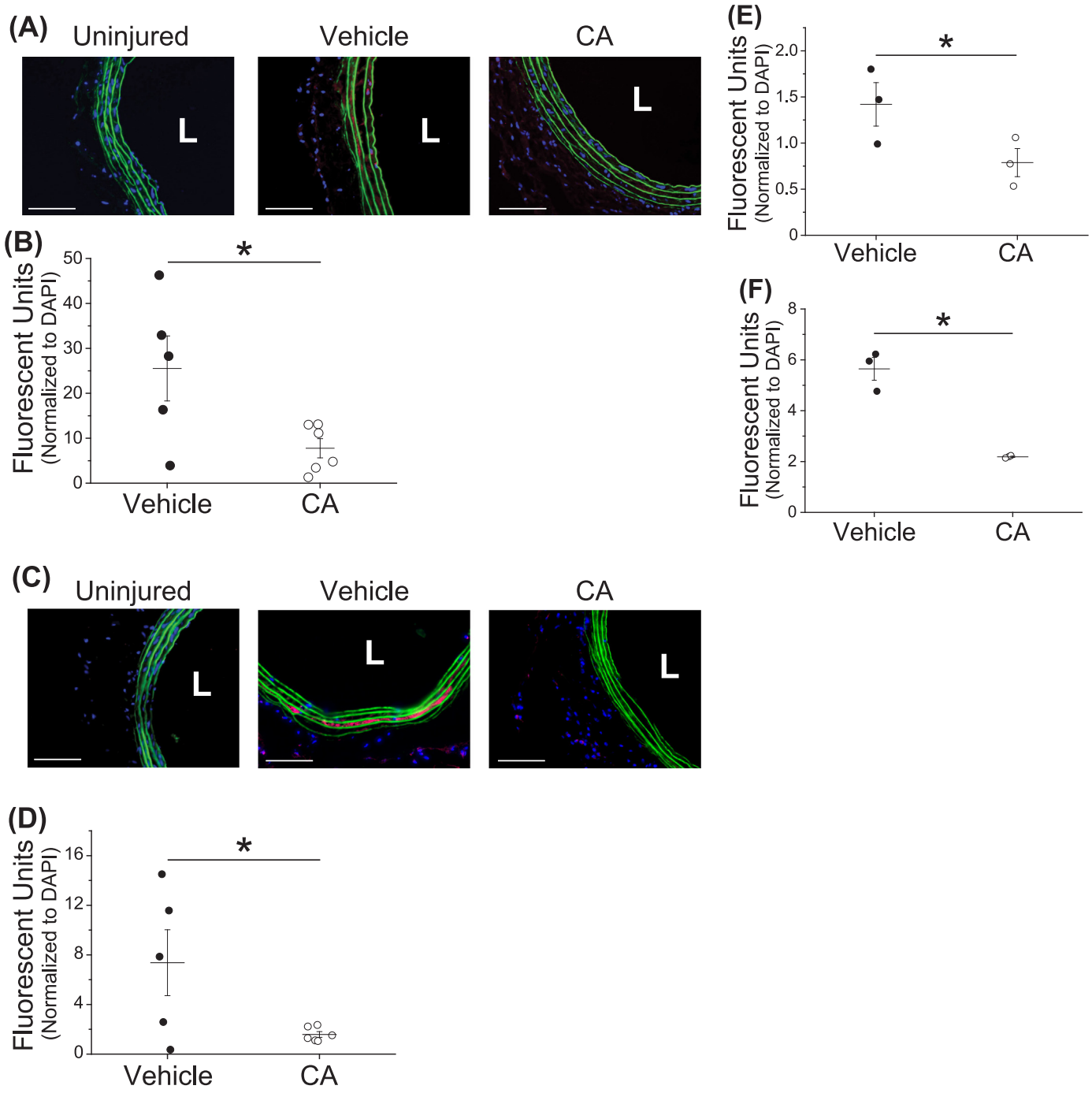

Fig. 6. Cinnamic aldehyde (CA) reduced immune cell invasion into the injured carotid artery. Hyperglycemic ZDF rats weighing 350–500 g underwent the carotid balloon injury and were treated with periadventitial application of Pluronic vehicle (100 μL) or CA in Pluronic (100 μM in 100 μL) at the time of surgery. Carotids were harvested three days or two weeks after surgery. (A) Myeloperoxidase (MPO) staining of uninjured and three-day injured carotid arteries treated with 100 μM CA or vehicle alone. Scale bar = 100 μm; Red = MPO; Blue = DAPI; Green = elastic lamina; L = lumen. (B) Quantification of MPO fluorescence from images in (A) normalized to cell nuclei (DAPI). (C) CD68 staining of three-day injured carotid arteries. Scale bar = 100 μm; Red = CD68 Blue = DAPI; Green = elastic lamina; L = lumen. (D) Quantification of CD68 staining from images in (C). (E) Quantification of CD68 fluorescence from two-week injured arteries of cohort 1. (F) Quantification of CD68 fluorescence from two-week injured arteries of cohort 2. *$p < 0.05$ compared to vehicle; Student's *t*-test. Each point indicates the average of three arterial cross-sections per rat (three-day injured: n = 5 for vehicle, n = 6 for CA; two-week injured: n = 3) with means ± SEM for each group overlaid.

regulated by Nrf2, which catalyzes the breakdown of hydrogen peroxide, a reactive species formed from superoxide reduction. 24-h treatment with CA and SFN increased the level of Prx1 in ZDF VSMC 2.2-fold and 1.8-fold respectively ($p < 0.05$, Fig. 4 A, F). Immunoblot for Prx3 showed no significant increase in enzyme levels following CA or SFN treatment for 24 h (data not shown). Together these assays highlight the ability of CA treatment to increase the levels and activity of enzymes regulating redox homeostasis.

Additionally, as a relative measure of redox dysfunction, we analyzed the level of fluorescence in PDGF-BB-stimulated ZDF VSMC and three-day injured ZDF carotid arteries stained with dihydroethidium (DHE). A significant 58% reduction in fluorescence was observed in VSMC treated for 24 h with 100 μM CA ($p < 0.05$, Fig. 5 A, B). Similarly, a significant 46% reduction in DHE fluorescence was observed in

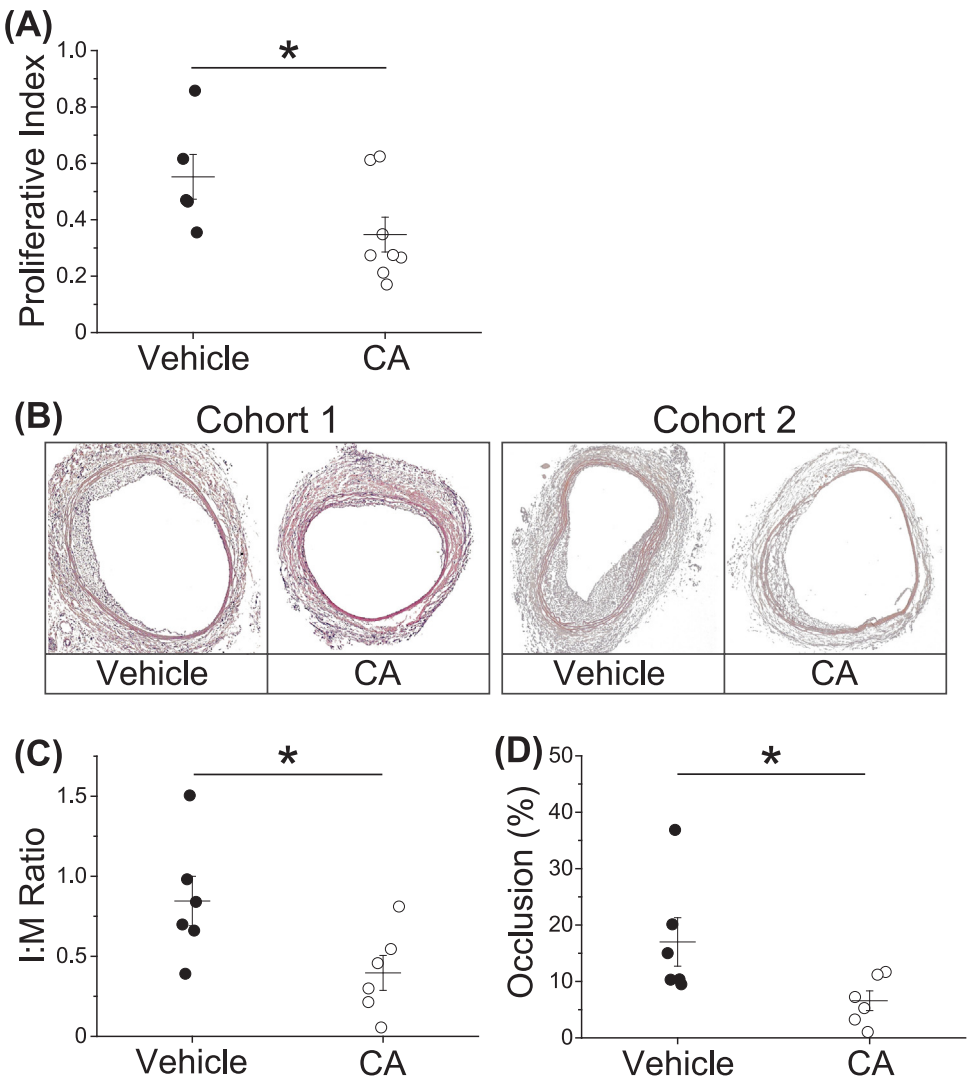

Fig. 7. Cinnamic aldehyde (CA) inhibited cellular proliferation in injured carotid arteries and the development of neointimal hyperplasia. Hyperglycemic ZDF rats weighing 350–500 g underwent the carotid balloon injury and were treated with periadventitial application of Pluronic vehicle (100 µL) or CA in Pluronic (100 µM in 100 µL) at the time of surgery. Carotids were harvested three days or two weeks after surgery. (A) Quantification of vessel proliferative index of three-day injured arteries by BrdU immunohistochemistry. (B) H &E stained arterial cross-sections of two-week injured rats from cohort 1 and cohort 2. (C) Quantification of the intima: media (I:M) ratio of carotid arteries from both cohorts in (B). (D) Quantification of percent vessel occlusion of carotid arteries from both cohorts in (B). *$p < 0.05$ compared to vehicle; Student's *t*-test. Each point indicates the average of three arterial cross-sections per rat (three-day injured: n = 5 for vehicle, n = 8 for CA; two-week injured: n = 6) with means ± SEM for each group overlaid.

the arteries of three-day injured ZDF rats treated with 100 µM CA compared to vehicle alone (Fig. 5C, D). Furthermore, we assessed 3-nitrotyrosine levels in the injured arteries as another marker of redox dysfunction. We found a significant 61% reduction in 3-nitrotyrosine staining within the injured arteries after treatment with 100 µM CA compared to vehicle alone ($p < 0.05$, Fig. 5 E, F). Taken together, these results suggest that 100 µM CA treatment at the time of injury reduced the local oxidative burden within ZDF VSMC and more broadly the injured ZDF rat carotid artery.

3.5. Cinnamic aldehyde reduces immune cell infiltration into injured carotid arteries

Local inflammation after vascular injury is an important driver of neointimal formation, therefore, we quantified the presence of immune cells in the carotid artery. Arteries from three-day injured rats were stained for myeloperoxidase (MPO) and CD68 as markers of neutrophil and macrophage presence respectively. Arteries treated with 100 µM CA had a 69% reduction in MPO staining compared to vehicle-treatment alone ($p < 0.05$, Fig. 6 A, B). Likewise, there was a significant 78% reduction in CD68 staining ($p < 0.05$, Fig. 6 C, D) suggesting CA treatment reduced neutrophil and macrophage infiltration into the injured carotid artery. Since macrophages play a role in both innate and adaptive immunity we also analyzed macrophage infiltration in the arteries of two-week injured rats. As we had two separate cohorts for the two-week injury time point we separated our analysis accordingly. Similar to the three-day time point, there was a significant 44% ($p < 0.05$, Fig. 6 E) and 61% ($p < 0.05$, Fig. 6 F) decrease in CD68 staining after CA treatment in cohort 1 and 2 respectively. Taken together, this suggests that CA reduced immune cell infiltration early after injury and this reduction persisted for up to two weeks during the vessel healing process.

3.6. Cinnamic aldehyde inhibits neointimal hyperplasia in the carotid artery after balloon injury

After seeing a reduction in ZDF VSMC number without increased death *in vitro* (Fig. 1), we evaluated the effects of 100 µM CA on proliferation of cells in the vessel wall of ZDF carotid arteries three days after balloon injury. Bromodeoxyuridine immunohistochemistry staining revealed a 37% reduction in total vessel proliferative index following 100 µM CA treatment ($p < 0.05$, Fig. 7 A). Thus, directly validating that CA can inhibit proliferation in our ZDF model.

As CA inhibited cell proliferation, redox dysfunction, and inflammation after arterial injury, we assessed its therapeutic potential at inhibiting restenosis after balloon injury. Analysis of two-week injured arteries from both injury cohorts stained with H&E (Fig. 7 B) showed that 100 µM CA effectively decreased neointimal hyperplasia. The I:M ratio was reduced by 53% from 0.85 ± 0.15 in the vehicle-treated group to 0.4 ± 0.11 in the CA-treated group ($p < 0.05$, Fig. 7 C). This

corresponded with a 61% decrease in the percent occlusion of the vessel from 17% ± 4.3% down to 6.6% ± 1.7% after CA treatment ($p < 0.05$, Fig. 7 D). This data suggests that CA effectively inhibits neointimal hyperplasia in a balloon injured diabetic rat model.

4. Discussion

Patients with DM have more extensive neointimal hyperplasia following revascularization procedures than non-diabetic individuals undergoing the same procedure [4–6]. VSMC are the main cell type within the vasculature to contribute to the development of neointimal hyperplasia. After injury VSMC undergo a phenotypic switch that leads to increased migration and proliferation towards the neointima. The ZDF rat is a well characterized and accepted model of type 2 DM. Therefore, we used ZDF VSMC cultured in 25 mM glucose supplemented with PDGF-BB and ZDF rats to test the potential therapeutic effect of CA in diabetic vascular restenosis. We have shown that 100 μM CA is a non-toxic dose that inhibits PDGF-BB-induced ZDF VSMC proliferation without causing apoptosis. Furthermore, CA was also capable of inhibiting PDGF-BB-induced migration. Utilizing BrdU incorporation, we noted inhibited cell proliferation within the balloon injured carotids of ZDF rats following local periadventitial CA treatment. Additionally, CA was able to induce Nrf2 nuclear translocation both *in vitro* and *in vivo* and induce canonical and non-canonical transcriptional targets of Nrf2 *in vitro*. Moreover, local application of CA inhibited markers of redox dysfunction *in vitro* and *in vivo*, as well as inflammatory cell infiltration in the ZDF rat carotid after balloon injury. Importantly, we found that local periadventitial application of CA inhibited neointimal hyperplasia development in ZDF rats two weeks after carotid balloon injury.

The effect of CA on cell proliferation has also been described by Zhou et al. who showed that CA inhibited proliferation of melanoma cells in a 3D skin culture model [33]. Additionally, Yoo et al. showed that SFN, the electrophile we used as a positive control for Nrf2 activation, also inhibited PDGF-BB-induced VSMC proliferation by inhibiting cell cycle progression [22]. Mechanistically, superoxide ($O_2^{\bullet-}$) production downstream of NOX1 has been postulated as an intracellular factor driving proliferation and migration of VSMC [12]. As CA has been previously reported to activate the Nrf2 pathway [26], we hypothesized that this activation could reduce redox dysfunction after arterial injury and inhibit restenosis. Indeed, we observed that CA treatment induced an increase in protein levels of HO-1, SOD-1, GCLC, and Prx1. Moreover, the increase in SOD1 protein resulted in a 1.6-fold increase in enzymatic activity, whereas the increase in GCLC resulted in increased intracellular GSH. Additionally, CA reduced DHE fluorescence in ZDF VSMC, suggesting CA mitigated the redox imbalance *in vitro*. Wang et al. showed that CA is capable of inducing translocation of Nrf2 to the nucleus and increasing protein expression of downstream enzymes in endothelial cells also cultured in hyperglycemic conditions [27]. They also went on to show that CA reduced DHE and 3-nitrotyrosine fluorescence of mouse aortic rings cultured in high glucose (30 mM) [27]. Similar to our *in vitro* probing and the findings from Wang et al., we saw nuclear colocalization of Nrf2 concomitantly with reduced DHE and 3-nitrotyrosine fluorescence and immunofluorescence respectively three days after balloon injury in ZDF rat carotids. This suggests that CA is capable of positively modulating the redox environment both *in vitro* and *in vivo* in our diabetic model by increasing antioxidant defenses.

Invading immune cells can negatively impact vessel remodeling and wound healing following revascularization and are a critical component of the arterial injury response leading to neointimal hyperplasia. Roth-Walter and Moskovskich et al. showed that CA exhibits immune suppressive effects by inhibiting proliferation and inducing apoptosis in primary immune cell lines even at 10 μM [34]. Furthermore, CA has been shown to inhibit secretion of pro-inflammatory cytokines [35] while promoting anti-inflammatory cytokine release [36] from macrophages *in vitro*. In our balloon injured ZDF carotid arteries we saw reduced presence of both neutrophils and macrophages and the aforementioned anti-inflammatory properties of CA may have contributed to this reduction in inflammatory cell number.

CA effectively inhibited neointimal hyperplasia at the two-week time point evidenced by a reduced I:M ratio and percent vessel occlusion. Similar to our results, Yoo et al. showed that the electrophile SFN was able to inhibit neointimal hyperplasia in a non-diabetic carotid artery balloon injury model [22]. Shawky and Segar showed that SFN inhibited VSMC proliferation and neointimal hyperplasia in a mouse femoral artery wire injury model [23]. This group has also previously shown that SFN is able to inhibit leptin-induced VSMC proliferation and suppress neointimal hyperplasia in diet-induced obese mice [24]. Together with our results these findings highlight the possibility of utilizing small electrophilic molecules as therapeutics for treating restenosis.

Despite the observed therapeutic efficacy this study has several limitations. Although our results showed a decrease in DHE fluorescence both *in vitro* and *in vivo*, this change cannot be attributed directly to a change in cellular levels of $O_2^{\bullet-}$ as there is significant overlap between the fluorescent emission of the $O_2^{\bullet-}$-specific product 2-hydroxyethidium and other DHE oxidation products [37]. However, we do see an increase in SOD-1 protein levels and activity in ZDF VSMC treated with CA to the same extent that has been previously shown to inhibit VSMC proliferation and reduce $O_2^{\bullet-}$ levels [30]. Of note, CA has been shown to inhibit xanthine oxidase (XO) [38], another enzyme responsible for $O_2^{\bullet-}$ production and for accelerating cardiovascular disease. However, there is conflicting evidence regarding the extent to which XO contributes to the increased $O_2^{\bullet-}$ production seen after vascular injury. Shi et al. showed that preincubation of uninjured pig coronary artery rings with XO inhibitor oxypurinol had no effect on $O_2^{\bullet-}$ production, as measured by the nitroblue tetrazolium assay, while preincubation with the NOX inhibitor diphenyleneiodonium completely abrogated $O_2^{\bullet-}$ production [39]. Meanwhile, Yamamoto et al. showed that the XO inhibitor allopurinol administered via drinking water for three weeks reduced the I:M ratio and neointimal area after carotid ligation in hypertensive rats [40]. Nevertheless, as XO has been broadly implicated to contribute to the pathogenesis of cardiovascular disease it is plausible that part of the therapeutic effect we see in our model is due to CA-mediated XO inhibition.

Another limitation of this study is that even though we show CA-induced activation of the Nrf2 pathway concomitant with a therapeutic effect we are not proving causality. As a reactive electrophile, CA could affect Nrf2-independent pathways by directly reacting with other cellular targets. CA may be inhibiting cell proliferation by targeting key pathways such as NF-kB [41], m-TOR [23], or the mitogen-activated protein kinase pathway [42,43] whose inhibition has been shown to prevent neointimal hyperplasia.

Work done by Zhou et al. showed that the CA-dependent inhibition of melanoma cell proliferation and invasion within the 3D skin culture model was paired with decreased matrix metalloproteinase-9 (MMP) expression [33]. Metalloproteinases, in particular MMP-9, have been shown to aid in VSMC migration during neointimal hyperplasia [12,44,45]. MMP9 production in VSMC depends on NOX1 activation [12]. Moreover, 8 weeks of oral exposure to a $O_2^{\bullet-}$ scavenger effectively reduces MMP-9 expression throughout the vasculature of spontaneously hypertensive rats [46]. These data agree with our observed inhibition of ZDF VSMC migration, and decrease of DHE fluorescence after CA treatment. Finally, CA has been extensively studied as a therapeutic to treat several non-vascular complications of diabetes in rodent models. Zhu and Liu et al. review these studies and highlight improved insulin sensitivity, glucose uptake, and lipid metabolism among the therapeutic benefits of CA across different rodent models of diabetes [29]. However, we treated the injured arteries locally to avoid systemic effects and therefore the therapeutic response we observed is most likely due to a direct effect of CA on the vascular wall.

5. Conclusion

CA increased antioxidant defenses *in vitro* while decreasing markers of redox dysfunction both *in vitro* and *in vivo*. To the best of our knowledge, this is the first study to show that local application of CA, an electrophilic small molecule capable of activating the Nrf2 pathway, to the injured artery is able to inhibit neointimal hyperplasia in a diabetic rat model. Our results, tohether with the literature, suggest that the therapeutic effect of CA after arterial injury may be through modulation of redox homeostasis via Nrf2.

Acknowledgments

The authors thank Dr. Hussein Kassam for training NEB on the balloon injury rat model, Dr. Brian C. Cooley and Ms. Megan Flynn for performing animal surgeries, as well as Ms. Robin Siletzky and Ms. Danielle Berlin for insight on improving this manuscript. NEB is supported by a training grant from the National Institute of Environmental Health Sciences (5T32ES007126-35, 2018). EMB is a KL2 scholar partially supported by the UNC Clinical and Translational Science Award-K12 Scholars Program funded by the National Center for Advancing Translational Sciences, US. (KL2TR002490, 2018). EMB is also supported by Institutional start-up funds, and a Nutrition and Obesity Research Center (NORC) Pilot and Feasibility Grant, funded by the National Institute of Diabetes and Digestive and Kidney Diseases, US (P30DK056350, 2018) from The University of North Carolina at Chapel Hill. Confocal microscopy was performed at the Northwestern University Center for Advanced Microscopy generously supported by the National Cancer Institute (CCSG 3P30CA060553-23S3, 2017).

Conflict of interest

The authors declare that there are no conflicts of interest regarding the publication of this manuscript.

References

[1] M. Writing Group, D. Mozaffarian, E.J. Benjamin, A.S. Go, D.K. Arnett, M.J. Blaha, et al., Executive summary: heart disease and stroke statistics–2016 update: a report from the American heart association, Circulation 133 (2016) 447–454.
[2] International Diabetes Federation Diabetes Atlas, Eighth edition, 2017.
[3] A.S. Matheus, L.R. Tannus, R.A. Cobas, C.C. Palma, C.A. Negrato, M.B. Gomes, Impact of diabetes on cardiovascular disease: an update, Int. J. Hypertens. 2013 (2013) 653789.
[4] C.P. Lexis, B.M. Rahel, J.G. Meeder, F. Zijlstra, I.C. van der Horst, The role of glucose lowering agents on restenosis after percutaneous coronary intervention in patients with diabetes mellitus, Cardiovasc. Diabetol. 8 (2009) 41.
[5] B.G. DeRubertis, M. Pierce, E.J. Ryer, S. Trocciola, K.C. Kent, P.L. Faries, Reduced primary patency rate in diabetic patients after percutaneous intervention results from more frequent presentation with limb-threatening ischemia, J. Vasc. Surg. 47 (2008) 101–108.
[6] M. Singh, R. Arora, V. Kodumuri, S. Khosla, E. Jawad, Coronary revascularization in diabetic patients: current state of evidence, Exp. Clin. Cardiol. 16 (2011) 16–22.
[7] S.O. Marx, H. Totary-Jain, A.R. Marks, Vascular smooth muscle cell proliferation in restenosis, Circ. Cardiovasc. Interv. 4 (2011) 104–111.
[8] S. Sartore, A. Chiavegato, E. Faggin, R. Franch, M. Puato, S. Ausoni, et al., Contribution of adventitial fibroblasts to neointima formation and vascular remodeling: from innocent bystander to active participant, Circ. Res. 89 (2001) 1111–1121.
[9] N.G. Kounis, I. Koniari, A. Roumeliotis, G. Tsigas, G. Soufras, N. Grapsas, et al., Thrombotic responses to coronary stents, bioresorbable scaffolds and the Kounis hypersensitivity-associated acute thrombotic syndrome, J. Thorac. Dis. 9 (2017) 1155–1164.
[10] L.C. Azevedo, M.A. Pedro, L.C. Souza, H.P. de Souza, M. Janiszewski, P.L. da Luz, et al., Oxidative stress as a signaling mechanism of the vascular response to injury: the redox hypothesis of restenosis, Cardiovasc. Res. 47 (2000) 436–445.
[11] P.F. Leite, M. Liberman, F. Sandoli, de Brito, F.R. Laurindo, Redox processes underlying the vascular repair reaction, World J. Surg. 28 (2004) 331–336.
[12] S. Xu, A.S. Shriver, D.K. Jagadeesha, A.H. Chamseddine, K. Szocs, N.L. Weintraub, et al., Increased expression of Nox1 in neointimal smooth muscle cells promotes activation of matrix metalloproteinase-9, J. Vasc. Res. 49 (2012) 242–248.
[13] K. Szocs, B. Lassegue, D. Sorescu, L.L. Hilenski, L. Valppu, T.L. Couse, et al., Upregulation of Nox-based NAD(P)H oxidases in restenosis after carotid injury, Arterioscler. Thromb. Vasc. Biol. 22 (2002) 21–27.
[14] M.Y. Lee, A. San Martin, P.K. Mehta, A.E. Dikalova, A.M. Garrido, S.R. Datla, et al., Mechanisms of vascular smooth muscle NADPH oxidase 1 (Nox1) contribution to injury-induced neointimal formation, Arterioscler. Thromb. Vasc. Biol. 29 (2009) 480–487.
[15] J. Streeter, W. Thiel, K. Brieger, F.J. Miller Jr., Opportunity nox: the future of NADPH oxidases as therapeutic targets in cardiovascular disease, Cardiovasc. Ther. 31 (2013) 125–137.
[16] A. Jawien, D.F. Bowen-Pope, V. Lindner, S.M. Schwartz, A.W. Clowes, Platelet-derived growth factor promotes smooth muscle migration and intimal thickening in a rat model of balloon angioplasty, J. Clin. Investig. 89 (1992) 507–511.
[17] Q.B. Lu, M.Y. Wan, P.Y. Wang, C.X. Zhang, D.Y. Xu, X. Liao, et al., Chicoric acid prevents PDGF-BB-induced VSMC dedifferentiation, proliferation and migration by suppressing ROS/NFkappaB/mTOR/P70S6K signaling cascade, Redox Biol. 14 (2018) 656–668.
[18] S. Pan, H. Lin, H. Luo, F. Gao, L. Meng, C. Zhou, et al., Folic acid inhibits dedifferentiation of PDGF-BB-induced vascular smooth muscle cells by suppressing mTOR/P70S6K signaling, Am. J. Transl. Res. 9 (2017) 1307–1316.
[19] H. Mao, T. Tao, D. Song, M. Liu, X. Wang, X. Liu, et al., Zedoarondiol inhibits platelet-derived growth factor-induced vascular smooth muscle cells proliferation via regulating AMP-activated protein kinase signaling pathway, Cell Physiol. Biochem. 40 (2016) 1506–1520.
[20] K. Itoh, T. Chiba, S. Takahashi, T. Ishii, K. Igarashi, Y. Katoh, et al., An Nrf2/small Maf heterodimer mediates the induction of phase II detoxifying enzyme genes through antioxidant response elements, Biochem. Biophys. Res. Commun. 236 (1997) 313–322.
[21] A. Raghunath, K. Sundarraj, R. Nagarajan, F. Arfuso, J. Bian, A.P. Kumar, et al., Antioxidant response elements: discovery, classes, regulation and potential applications, Redox Biol. 17 (2018) 297–314.
[22] S.H. Yoo, Y. Lim, S.J. Kim, K.D. Yoo, H.S. Yoo, J.T. Hong, et al., Sulforaphane inhibits PDGF-induced proliferation of rat aortic vascular smooth muscle cell by up-regulation of p53 leading to G1/S cell cycle arrest, Vasc. Pharmacol. 59 (2013) 44–51.
[23] N.M. Shawky, L. Segar, Sulforaphane inhibits platelet-derived growth factor-induced vascular smooth muscle cell proliferation by targeting mTOR/p70S6kinase signaling independent of Nrf2 activation, Pharmacol. Res. 119 (2017) 251–264.
[24] N.M. Shawky, P. Pichavaram, G.S. Shehatou, G.M. Suddek, N.M. Gameil, J.Y. Jun, et al., Sulforaphane improves dysregulated metabolic profile and inhibits leptin-induced VSMC proliferation: implications toward suppression of neointima formation after arterial injury in western diet-fed obese mice, J. Nutr. Biochem. 32 (2016) 73–84.
[25] C.M. Cabello, W.B. Bair 3rd, S.D. Lamore, S. Ley, A.S. Bause, S. Azimian, et al., The cinnamon-derived michael acceptor cinnamic aldehyde impairs melanoma cell proliferation, invasiveness, and tumor growth, Free Radic. Biol. Med. 46 (2009) 220–231.
[26] G.T. Wondrak, N.F. Villeneuve, S.D. Lamore, A.S. Bause, T. Jiang, D.D. Zhang, The cinnamon-derived dietary factor cinnamic aldehyde activates the Nrf2-dependent antioxidant response in human epithelial colon cells, Molecules 15 (2010) 3338–3355.
[27] F. Wang, C. Pu, P. Zhou, P. Wang, D. Liang, Q. Wang, et al., Cinnamaldehyde prevents endothelial dysfunction induced by high glucose by activating Nrf2, Cell Physiol. Biochem. 36 (2015) 315–324.
[28] H.M. El-Bassossy, A. Fahmy, D. Badawy, Cinnamaldehyde protects from the hypertension associated with diabetes, Food Chem. Toxicol. 49 (2011) 3007–3012.
[29] R. Zhu, H. Liu, C. Liu, L. Wang, R. Ma, B. Chen, et al., Cinnamaldehyde in diabetes: a review of pharmacology, pharmacokinetics and safety, Pharmacol. Res. 122 (2017) 78–89.
[30] E.S. Bahnson, N. Koo, N. Cantu-Medellin, A.Y. Tsui, G.E. Havelka, J.M. Vercammen, et al., Nitric oxide inhibits neointimal hyperplasia following vascular injury via differential, cell-specific modulation of SOD-1 in the arterial wall, Nitric Oxide 44 (2015) 8–17.
[31] Y. Bai, X. Wang, S. Zhao, C. Ma, J. Cui, Y. Zheng, Sulforaphane Protects against Cardiovascular Disease via Nrf2 Activation, Oxid. Med Cell Longev. 2015 (2015) 407580.
[32] H. Dreger, K. Westphal, N. Wilck, G. Baumann, V. Stangl, K. Stangl, et al., Protection of vascular cells from oxidative stress by proteasome inhibition depends on Nrf2, Cardiovasc. Res. 85 (2010) 395–403.
[33] L. Zhou, Y. Lu, J. Wu, G. Yang, T. Yang, Cinnamic aldehyde inhibits proliferation and invasion in a well-defined 3-dimensional culture of human cutaneous melanoma cells in tissue engineered-skin, Asian Biomed. 7 (2013) 145–153 (April 2013).
[34] F. Roth-Walter, A. Moskovskich, C. Gomez-Casado, A. Diaz-Perales, K. Oida, J. Singer, et al., Immune suppressive effect of cinnamaldehyde due to inhibition of proliferation and induction of apoptosis in immune cells: implications in cancer, PLoS One 9 (2014) e108402.
[35] L.K. Chao, K.F. Hua, H.Y. Hsu, S.S. Cheng, I.F. Lin, C.J. Chen, et al., Cinnamaldehyde inhibits pro-inflammatory cytokines secretion from monocytes/macrophages through suppression of intracellular signaling, Food Chem. Toxicol. 46 (2008) 220–231.
[36] C. Pannee, I. Chandhanee, L. Wacharee, Antiinflammatory effects of essential oil from the leaves of Cinnamomum cassia and cinnamaldehyde on lipopolysaccharide-stimulated J774A.1 cells, J. Adv. Pharm. Technol. Res. 5 (2014) 164–170.
[37] J. Zielonka, B. Kalyanaraman, Hydroethidine- and MitoSOX-derived red fluorescence is not a reliable indicator of intracellular superoxide formation: another inconvenient truth, Free Radic. Biol. Med. 48 (2010) 983–1001.
[38] S.Y. Wang, C.W. Yang, J.W. Liao, W.W. Zhen, F.H. Chu, S.T. Chang, Essential oil from leaves of Cinnamomum osmophloeum acts as a xanthine oxidase inhibitor and reduces the serum uric acid levels in oxonate-induced mice, Phytomedicine 15

(2008) 940–945.
[39] Y. Shi, R. Niculescu, D. Wang, S. Patel, K.L. Davenpeck, A. Zalewski, Increased NAD(P)H oxidase and reactive oxygen species in coronary arteries after balloon injury, Arterioscler. Thromb. Vasc. Biol. 21 (2001) 739–745.
[40] Y. Yamamoto, K. Ogino, G. Igawa, T. Matsuura, Y. Kaetsu, S. Sugihara, et al., Allopurinol reduces neointimal hyperplasia in the carotid artery ligation model in spontaneously hypertensive rats, Hypertens. Res. 29 (2006) 915–921.
[41] H.J. Sun, M.X. Zhao, X.S. Ren, T.Y. Liu, Q. Chen, Y.H. Li, et al., Salusin-beta promotes vascular smooth muscle cell migration and intimal hyperplasia After vascular injury via ROS/NFkappaB/MMP-9 pathway, Antioxid. Redox Signal. 24 (2016) 1045–1057.
[42] P.R. Kapopara, J. von Felden, O. Soehnlein, Y. Wang, L.C. Napp, K. Sonnenschein, et al., Deficiency of MAPK-activated protein kinase 2 (MK2) prevents adverse remodelling and promotes endothelial healing after arterial injury, Thromb. Haemost. 112 (2014) 1264–1276.
[43] J. Gan, P. Li, Z. Wang, J. Chen, X. Liang, M. Liu, et al., Rosuvastatin suppresses platelet-derived growth factor-BB-induced vascular smooth muscle cell proliferation and migration via the MAPK signaling pathway, Exp. Ther. Med. 6 (2013) 899–903.
[44] N. Zempo, N. Koyama, R.D. Kenagy, H.J. Lea, A.W. Clowes, Regulation of vascular smooth muscle cell migration and proliferation in vitro and in injured rat arteries by a synthetic matrix metalloproteinase inhibitor, Arterioscler. Thromb. Vasc. Biol. 16 (1996) 28–33.
[45] J.L. Johnson, A. Dwivedi, M. Somerville, S.J. George, A.C. Newby, Matrix metalloproteinase (MMP)-3 activates MMP-9 mediated vascular smooth muscle cell migration and neointima formation in mice, Arterioscler. Thromb. Vasc. Biol. 31 (2011) e35–e44.
[46] N. Duansak, G.W. Schmid-Schonbein, The oxygen free radicals control MMP-9 and transcription factors expression in the spontaneously hypertensive rat, Microvasc. Res. 90 (2013) 154–161.